Acta Mech 229, 1275–1295 (2018)
https://doi.org/10.1007/s00707-017-2059-1

ORIGINAL PAPER

N. Jamia · P. Rajendran · S. El-Borgi · M. I. Friswell

Mistuning identification in a bladed disk using wavelet packet transform

Received: 6 June 2017 / Revised: 14 October 2017 / Published online: 15 November 2017

Abstract The dynamic response of a bladed disk is very sensitive to the symmetry of identical blades. If the properties of one or more blades vary slightly then the response can increase substantially, which is known as mistuning. Mistuning in bladed disks due to manufacturing tolerances has been extensively studied, with emphasis on response and fatigue life prediction. Damage to blades can also cause mistuning but has received only limited attention. The identification of mistuning in rotating bladed disks is a challenging and an ongoing topic of investigation. This study proposes a Wavelet Energy-Based Mistuning Index (WEBMI) which is obtained from the wavelet packet transforms of both tuned and mistuned blade responses, and requires only output response signals. The proposed mistuning index is demonstrated on a lumped parameter model of a bladed disk, and mistuning was represented by altering the stiffness or mass of individual blades. Mistuning to single and multiple blades with different locations and severities was simulated. Gaussian white noise was added to the response signal to test robustness. Finally, experiments were conducted to validate the feasibility of the proposed method. The results demonstrate that the WEBMI is sensitive enough to identify subtle mistuning as small as 0.5% in single and multiple locations. Furthermore, the mistuning index increases monotonically with increases in mistuning severity.

1 Introduction

Gas turbines are extremely used in the oil and gas industries. Previous studies have reported that around 42% of gas turbine failures occur due to faults in blades [1]. One of the most-encountered problems in gas turbines is the so-called mistuning which is essentially a bladed disk with nonidentical blades. This may be due to variations in material properties or manufacturing tolerances or scatter in blade geometry or blade damage due to cracks. It was shown that mistuning can significantly amplify the dynamic response of a bladed disk [2] resulting in potentially catastrophic high-cycle fatigue failures.

Generally, solving mistuning problems in bladed disks needs an accurate model to provide the dynamic behavior of the blades. Many researchers have used finite element (FE) models to investigate mistuning in bladed disks. Although an FE model can be generated for one sector of a bladed disk, cyclic symmetry routines

N. Jamia · M. I. Friswell
Swansea University, Bay Campus, Fabian Way, Swansea SA1 8EN, UK

P. Rajendran · S. El-Borgi (✉)
Mechanical Engineering Program, Texas A&M University at Qatar, Engineering Building, P.O. Box 23874, Education City, Doha, Qatar
E-mail: sami.el_borgi@qatar.tamu.edu
Tel.: +974 4423 0674

P. Rajendran
School of Mechanical Engineering, SASTRA University, Thanjavur, Tamil Nadu 613 401, India

cannot be used to predict the effect of mistuning, which destroys the required symmetry; therefore, a full model is needed. The vibration response of bladed disks used in turbines and the corresponding behavior caused by mistuning phenomena were predicted by Imergun and Ewins [3] and Rzadkowski [4] using full FE models. Due to the high computational cost of these simulations, techniques are used to generate a reduced-order model (ROM) for a single sector of the bladed disk. Castanier and Pierre [2] presented a review on mistuned bladed disks, where they summarized the different studies on reduced-order modeling performed over the last two decades. They showed that sector mistuning models using the FE approach can provide higher accuracy in the blade dynamic response. Luo [5] investigated the effect of adjacent blades on the modal parameters of bladed disks using elastic hinge theory. An analytical expression was proposed for the blade response, which gave a good approximation for the loads, but only a moderate approximation for the natural frequencies, when compared to a detailed finite element model. A basic model of a bladed disk is represented by a spring–mass system with either one or two degrees of freedom (DOF) for each sector, called a lumped parameter model. An amplified vibration response due to mistuning can be demonstrated on a model with a single degree of freedom (SDOF) per blade. Guerra and Mingolet [6] showed that the presence of strong coupling between the blades could not avoid the amplification of the vibration response of a mistuned bladed disk. They used the special case of a SDOF per blade disk model based on the reduced-order model of a blisk to study the parametric behavior [7]. Recently, in addition to blade damage, Chatterjee and Kotambkar [8] and Chatterjee [9] focused on the effect of the mistuning on the modal spectrum due to lacing wire damage. They used a SDOF lumped spring–mass system coupled with spring elements representing the lacing wire. However, the SDOF model provides the coupling between the blades through lacing wires but not coupling through the disk sectors. Therefore, Salhi et al. [10,11] proposed a two DOF model which represents the motion of the blades and disk sectors. In this model, one DOF per sector represents the disk and allows coupling between the disk sectors. Yao et al. [12] computed the nonlinear steady-state response of rotating, thin-walled, pre-twisted compressor blades of gas turbine engines and utilized the Galerkin approach to discretize the governing partial differential equation of motion to a two DOF system. The review of Yuan et al. [13] showed that the two DOF model has been widely used at the initial stage of design since it can capture the fundamental dynamics of the bladed disk.

During the last decade, researchers have focused on specific mistuning caused by blade cracking based on modal parameters and blade tip timing signals. Hou [14] investigated the effect on the first natural frequency and the first mode shape of different mistuned blades. Guru et al. [15] identified rotor blade damage from a sudden drop in the natural frequency beyond the allowable scatter and an abrupt change in the blade tip position. Wang et al. [16] investigated the effects of mistuning and cracks on the resonant frequencies of a mistuned impeller with a crack. However, a shift in natural frequencies sometimes occurred due to improper sampling rates and measurement errors which may lead to false identification. These studies highlight that modal parameters are not sensitive indicators of damage induced mistuning. Hanachi et al. [17] proposed a technique for crack detection in an engine bladed disk by detrended fluctuation analysis using blade tip clearance and time-of-arrival signals. Madhavan et al. [18] focused on detecting blade damage by observing the abnormalities in the vibration characteristics of the blade tip timing data measurements during engine tests. Identifying damage from only the response time signal is a great challenge.

Signal amplification techniques are necessary to enhance the mistuning features due to subtle changes in the signal from the bladed disk. The short time Fourier transform (STFT) was introduced to concentrate the signal in a time–frequency window, and this approach can handle non-stationary signals [19]. However, the STFT provides a fixed resolution because it is associated with a fixed width window function. To overcome this issue, the wavelet transform (WT) was proposed, which has an adjustable window in time/space–frequency. The continuous wavelet transform (CWT) provides localization features between the time/space and frequency domains, and has the ability to magnify subtle changes that exist in a signal. The CWT was applied to mode shapes to identify various damage locations and their depths in beam and plate structures [20–22]. However, mode shapes require a high density of measurement points to detect small changes due to damage. More recently, the discrete wavelet transform (DWT) was proposed to overcome the deficiency of the CWT. The DWT requires discrete sampling and consists of one high-frequency component from every level and one low-frequency component at the last level. The DWT has detected abrupt changes in seismic vibration responses by the analysis of displacement or velocity responses [23]. Nonetheless, the DWT fails to predict small changes in the high-frequency component due to the incomplete decomposition of a signal. WPT is an advanced signal processing tool which takes complete decomposition, including both low-frequency (approximate) and high-frequency (detailed) components. The result produces a fine frequency resolution in the high-frequency domain which is able to predict small changes in a signal. The WPT was applied to rotational mode shapes to identify

the added mass locations in beam and plate structures by numerical simulation [24,25]. However, it is difficult to extract the mode shapes, and a method using the vibration time signal directly is desirable. Han et al. [26] obtained the time signal from a simply supported beam and then applied the WPT to detect structural damage.

From the above review, the following points can be concluded: (a) a two DOF model of a bladed disk is sufficient to predict the machine dynamics, in particular to investigate the mistuning effects of blades; (b) modal parameters are insensitive to damage, and using the time response for damage or mistuning identification is preferable; (c) the WPT provides high resolution at high frequencies in comparison with the STFT, CWT, and DWT. Furthermore, to the best of the authors' knowledge, the WPT has not been used to identify mistuning in a bladed disk. Hence, the novelty of this study is to (i) apply the WPT to identify mistuned blades and severities; (ii) develop a WEBMI capable of capturing minute mistuning severity in the order of 0.5%, and (iii) validate the robustness of the proposed methodology both numerically and experimentally.

The paper is arranged as follows. Section 2 describes the basic underlying theory behind the WPT and the formulation of the proposed WEBMI. Numerical and experimental results are presented and discussed in Sects. 3 and 4, respectively. Finally, a summary of this study and concluding remarks are provided in Sect. 5.

2 Wavelets for damage identification

2.1 Theoretical background of the WPT

The WPT is an extended version of the DWT, which provides a complete level-by-level decomposition of the signal. Each node of every level is split into approximate and detail coefficients as shown in Fig. 1. In the WPT, the wavelet packets consist of a linear combination of the usual wavelet functions. They inherit some key properties such as orthonormality, invertibility, and time–frequency localization from their corresponding wavelet functions. The wavelet packet $\psi^i_{j,k}$ is a function where i, j, and k are the frequency modulation, scale (decomposition level) and translation parameters, respectively. Thus,

$$\psi^i_{j,k} = 2^{j/2}\psi^i(2^j t - k). \tag{1}$$

The wavelet functions ψ^i can be generated by a recursive relationship as

$$\psi^{2i}(t) = \sqrt{2}\sum_{k=0}^{T} h(k)\psi^i(2t-k), \tag{2.1}$$

$$\psi^{2i+1}(t) = \sqrt{2}\sum_{k=0}^{T} g(k)\psi^i(2t-k). \tag{2.2}$$

The first wavelet function is known as the mother wavelet, and thus

$$\psi^1(t) = \psi(t). \tag{3}$$

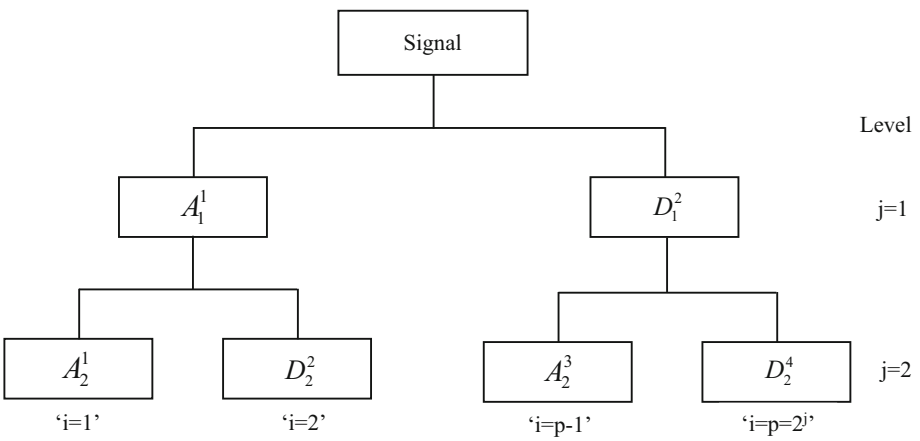

Fig. 1 Wavelet packet decomposition tree

The discrete filters $h(k)$ and $g(k)$ are the quadrature mirror filters associated with the scaling function and the mother wavelet function. The WPT consists of complete decomposition at every level and thus can achieve a higher resolution in the high-frequency region. The recursive relations between the jth and the $(j+1)$th level components are

$$f_j^i(t) = f_{j+1}^{2i-1}(t) + f_{j+1}^{2i}(t), \tag{4.1}$$

$$f_{j+1}^{2i-1}(t) = Hf_j^i(t), \tag{4.2}$$

$$f_{j+1}^{2i}(t) = Gf_j^i(t) \tag{4.3}$$

where H and G are the filtering-decimation operators related to the discrete filters $h(k)$ and $g(k)$ such that

$$H\{\cdot\} = \sum_{k=0}^{T} h(k-2t), \tag{5.1}$$

$$G\{\cdot\} = \sum_{k=0}^{T} g(k-2t). \tag{5.2}$$

After the jth level of decomposition, the original signal $f(t)$ can be expressed as

$$f(t) = \sum_{i=1}^{2^j} f_j^i(t). \tag{6}$$

The wavelet packet component signal $f_j^i(t)$ can be represented by a linear combination of the wavelet packet functions $\psi_{j,k}^i(t)$ as

$$f_j^i(t) = \sum_{k=0}^{T} C_{j,k}^i(t) \cdot \psi_{j,k}^i(t) \tag{7}$$

where the wavelet packet coefficients $C_{j,k}^i$ can be obtained from

$$C_{j,k}^i = \int_0^T f(t)\psi_{j,k}^i(t)\mathrm{d}t, \tag{8}$$

$$C_{j,k}^i = A_{j,k}^i, \quad \text{if} \quad i = 1, 3, 5\ldots \tag{9}$$

$$C_{j,k}^i = D_{j,k}^i, \quad \text{if} \quad i = 2, 4, 6\ldots \tag{10}$$

where $A_{j,k}^i$ and $D_{j,k}^i$ are the approximate and detail coefficients, respectively. The wavelet packet functions are assumed to be orthogonal, that is

$$\int_0^T \psi_{j,k}^r(t)\ \psi_{j,k}^q(t)\,\mathrm{d}t = 0, \quad \text{if } r \neq q. \tag{11}$$

2.2 Wavelet Energy-Based Mistuning Index (WEBMI)

The vibration signals are subjected to a WPT analysis, and a wavelet packet node energy index is estimated via the wavelet packet coefficients. Numerical simulations are performed on the rotating blades under rotating speed excitation. The various levels of mistuning assessment including the existence, location, and severity of the mistuning are studied. Here, the WEBMI is proposed to identify the location and severity of mistuning. Thus, the wavelet packet energy E of the jth level at the ith nodal component can be considered as the energy stored in the packet signal $f_j^i(t)$ and is given by

$$E_j^i = \int_0^T f_j^i(t)^2\mathrm{d}t. \tag{12}$$

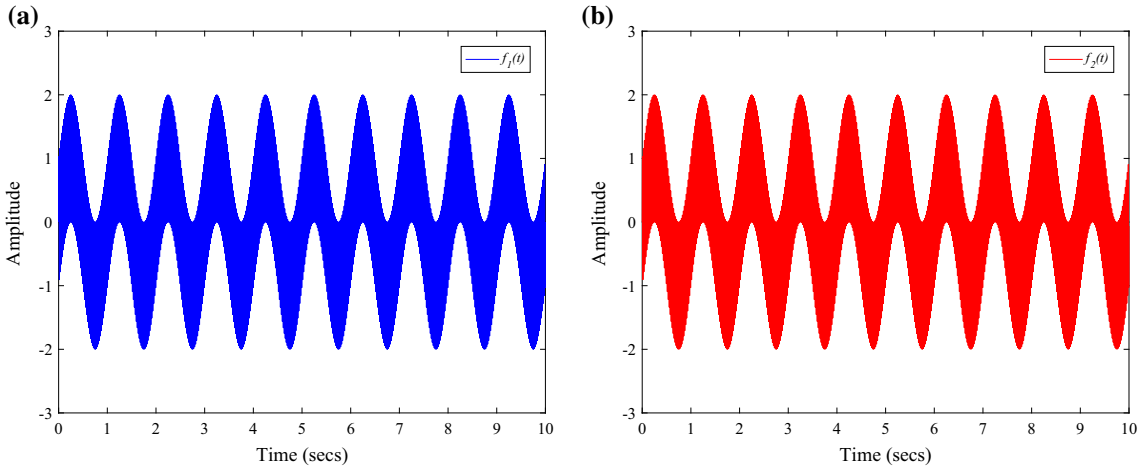

Fig. 2 Sinusoidal signal function

The component signal $f_j^i(t)$ is extracted from the jth level but is translated in the time domain so that $0 < t < T$. The estimated component energy E_j^i is the energy stored in different frequency bands at the jth scale. The relative change of the signal wavelet packet energy ΔE at the jth level and the ith node is defined as

$$\Delta E_j^i = \frac{\left|\left(E_j^i\right)_{\mathrm{d}} - \left(E_j^i\right)_{\mathrm{u}}\right|}{\left(E_j^i\right)_{\mathrm{u}}} \tag{13}$$

where the subscripts d and u denote the damaged and undamaged cases, respectively.

2.3 Case study

Each packet in a WPT tree may be considered as a filter, and thus the entire tree is essentially a filter bank. At higher levels of decomposition, the WPT yields a fine resolution in the frequency domain, although with a poor resolution in the time domain. To demonstrate the WPT, and that the high-frequency packets are more sensitive to subtle changes, consider the sinusoidal signals given by

$$f_1(t) = \sin(4\pi t) + \sin(100\pi t), \tag{14.1}$$
$$f_2(t) = \sin(4\pi t) + \sin(99.98\pi t). \tag{14.2}$$

The sinusoidal signal f_1 consists of two frequencies at 2 and 100 Hz for a duration of 5 s as shown in Fig. 2a. A small perturbation is introduced by reducing the high-frequency component by 0.01 Hz in the original signal to give f_2, which has the same duration as shown in Fig. 2b. The small frequency change is not visible in the time signal. Thus, the signal is passed through the filter bank of the WPT, and the small changes are captured by the third and fourth levels of decomposition. The corresponding WPT nodal energy values are given in Table 1. Typically, the last frequency packet energy change at the pth node is sensitive to the subtle change of 0.01 Hz, as shown in levels 3 and 4 given Table 1.

Therefore, only the last node, or the pth nodal energy change, is selected, and this method is termed the WEBMI. This approach is proposed to identify the subtle changes in the response signal that occur due to mistuning in different blades. Thus,

$$\Delta E_j^p = \frac{\left|\left(E_j^p\right)_{\mathrm{d}} - \left(E_j^p\right)_{\mathrm{u}}\right|}{\left(E_j^p\right)_{\mathrm{u}}}. \tag{15}$$

The detailed methodology of mistuning identification using the WPT analysis is illustrated by the flowchart shown in Fig. 3.

Table 1 The energy change at different packets of the third level and fourth levels of decomposition

Level $j=3$	$f(t)$	$f_3^1(t)$	$f_3^2(t)$	$f_3^3(t)$	$f_3^4(t)$	$f_3^5(t)$	$f_3^6(t)$	$f_3^7(t)$	$f_3^8(t)$
$\Delta E_3\%$	0.0009	0.0037	0.0111	0.0101	0.0007	0.0099	0.0009	0.0019	**0.0192**
Level $j=4$	$f(t)$	$f_4^1(t)$	$f_4^2(t)$	$f_4^3(t)$	$f_4^4(t)$	$f_4^5(t)$	$f_4^6(t)$	$f_4^7(t)$	$f_4^8(t)$
$\Delta E_4\%$	0.0009	0.001	0.0093	0.0197	0.0144	0.0204	0.0133	0.0015	0.0009
Level $j=4$	$f_4^9(t)$	$f_4^{10}(t)$	$f_4^{11}(t)$	$f_4^{12}(t)$	$f_4^{13}(t)$	$f_4^{14}(t)$	$f_4^{15}(t)$	$f_4^{16}(t)$	
$\Delta E_4\%$	0.0205	0.0131	0.0013	0.0011	0.0003	0.0021	0.0139	**0.0227**	

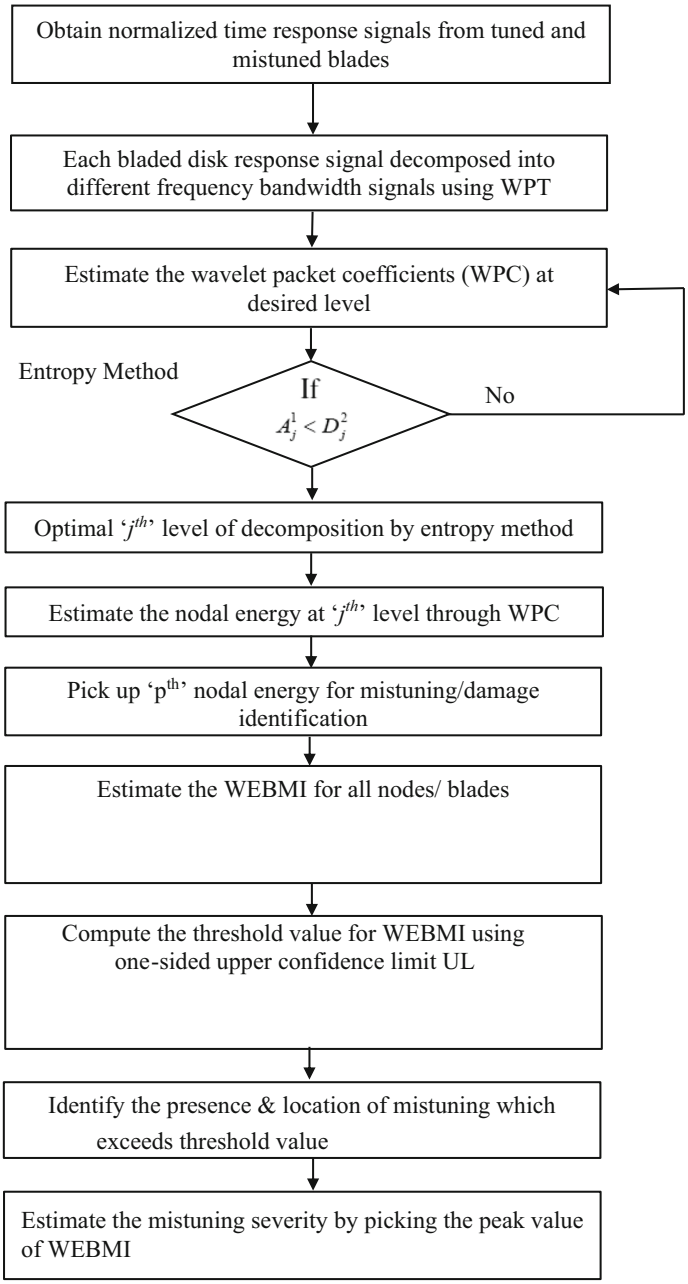

Fig. 3 Mistuning identification methodology

2.4 Selection of wavelet parameters

2.4.1 Selection of wavelet function

The optimal wavelet is chosen to detect subtle changes in the time signal. The localization property of the wavelet provides a filter to extract interesting characteristics such as energy in the time-scale signals. The Haar wavelet is chosen since it is highly discontinuous; the mother wavelet can be expressed by [27]

$$\psi = \begin{cases} 1 & 0 < t < 1/2 \\ -1 & 1/2 < t < 1 \\ 0 & \text{otherwise.} \end{cases} \tag{16}$$

This wavelet function tends to emphasize the discontinuities in the raw time signal. Note that the 'db1' wavelet is equivalent to the 'Haar' wavelet. Thus, the discontinuous Haar wavelet is used to detect damage or mistuning features in the time signal.

2.4.2 Selection of the level of decomposition

Entropy is a quantitative measure of how much uncertainty is contained in the signal. This particular property is useful to decide the optimal level of decomposition. Thus, the Shannon entropy (non-normalized) is employed to extract the features from different energy quality signals. Let the signal be $f = \{f_j : j = 1, 2, 3 \ldots N\}$. The Shannon (non-normalized) entropy of the jth level is represented as [28]

$$SE_j = \sum_{i=0}^{p} E_j^i \log E_j^i \tag{17}$$

where E_j^i is the wavelet packet energy at level j and node i. The wavelet packet energy for the approximate and detailed coefficients at each decomposition level is obtained as

$$EA_j^i = |A_j^i|^2 \tag{18}$$

and

$$ED_j^i = |D_j^i|^2, \tag{19}$$

in which $j = 1, 2, 3, \ldots, J$, and J represents the total number of decomposition levels. EA_j^i and ED_j^i are the energy packets for the approximate, A_j^i, and detailed, D_j^i, coefficients, respectively. To determine the optimal level of decomposition, the entropy of the signal is computed at each node of the jth decomposition level as shown in Fig. 1. However, most of the information is contained in the approximation coefficients in the wavelet packet transform signal. Therefore, the decomposition level at which the entropy of the approximation coefficients, EA_j^1, becomes less than that of the detailed coefficients, ED_j^2, is considered as optimal level of decomposition.

2.5 Threshold

In order to provide an alarm for the presence of damage, a threshold is established using the statistical properties and the one-sided confidence limit of the damage indicators from successive measurements. If N is the total number of sensors placed on the bladed disk, a total of N WEBMIs can be obtained after performing the wavelet packet decomposition. The mean and standard deviation of these WEBMIs is expressed as μ_{WEBMI} and σ_{WEBMI}, respectively. Therefore, the one-sided upper confidence limit for the WEBMI can be obtained as [29]

$$\text{UL}_{\text{WEBMI}}^{\alpha} = \mu_{\text{WEBMI}} + Z_{\alpha}\left(\frac{\sigma_{\text{WEBMI}}}{\sqrt{N}}\right) \tag{20}$$

where Z_{α} is the value of the standard normal distribution with zero mean and unit variance such that the cumulative probability is $100\ (1-\alpha)\%$. This upper limit can be considered as a threshold value and therefore as an alarm for possible abnormality in the damage indicator WEBMI. Any index that exceeds the threshold would cause the damage alarm to trigger.

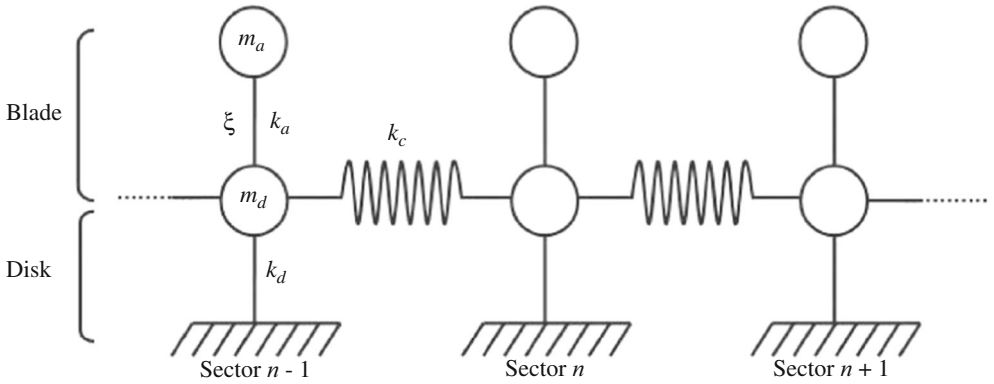

Fig. 4 Two degrees of freedom per sector model [11]

3 Numerical simulation

The numerical simulation is performed on a reduced-order two DOF model of the bladed disk developed by [11] and briefly summarized in Sect. 3.1. The bladed disk is composed of 20 blades. An impulse is applied to any blade and subsequently the corresponding time response is obtained from each blade tip. The output-only response signal is used for the WPT analysis, and the Daubechies 'db1' or 'Haar' wavelet is found to be effective for this study as discussed in Sect. 2.4.1. The optimal level of decomposition is chosen by the Shannon entropy method based on the signal characteristics, as briefly discussed in Sect. 2.4.2. The multiple test cases given in Table 3 have been simulated for single and multiple mistuned blades, and with and without noise.

3.1 Modeling of the dynamics of a bladed disk

The two DOF per sector model of a rotating bladed disk is discussed based on the model provided by Salhi et al. [11]. This basic model predicts some of the fundamental dynamics of bladed disks. Figure 4 shows a schematic of the model, where only three sectors of the bladed disk are represented as a mass–spring system. This model has two DOF per sector, representing the blade and the disk sector. Each disk sector is coupled to the neighboring sectors by the stiffness k_c. The stiffness of an individual blade is represented by k_a. It is assumed that each blade in the assembly has one significant mode which is typically the first bending mode. No centrifugal stiffening or rotational dynamics effects are considered explicitly in this model, although centrifugal stiffening could be included by increasing the blade stiffness k_a. A proportional damping model is assumed. A bladed disk assembly with 20 blades is simulated to investigate the mistuning effects due to damage in a bladed disk. A free vibration response of each blade and disk sector is generated.

The equation of motion of the bladed disk model in free vibration is defined as

$$\mathbf{M}\ddot{\mathbf{q}}(t) + \mathbf{C}\dot{\mathbf{q}}(t) + \mathbf{K}\mathbf{q}(t) = 0 \tag{21}$$

where $\mathbf{q}(t)$ is the vector of displacements corresponding to (2×20) DOF. The displacement of the nth sector is given by

$$\mathbf{q}^n(t) = \begin{bmatrix} q_1^n(t) \\ q_2^n(t) \end{bmatrix} \tag{22}$$

where the subscripts 1 and 2 represent the blade and the disk sector, respectively. The displacement for all sectors is then given by the global (40×1) vector

$$\mathbf{q}(t) = \begin{bmatrix} \mathbf{q}^1(t) \\ \vdots \\ \mathbf{q}^{40}(t) \end{bmatrix}. \tag{23}$$

Table 2 Properties of the bladed disk

m_a	1 kg
m_d	1 kg
k_a	10 kN/m
k_d	20 kN/m
k_c	0.2 k_a kN/m
n_b	20

M, **C**, and **K** represent the structural mass, damping, and stiffness matrices of dimension $N \times N$ with $N = 2n_b = 40$, where n_b is the number of blades. The mass matrix is given by

$$\mathbf{M} = \begin{bmatrix} \mathbf{M_s} & \mathbf{0} & \mathbf{0} & \cdot & \mathbf{0} \\ \mathbf{0} & \mathbf{M_s} & \mathbf{0} & \cdot & \mathbf{0} \\ \mathbf{0} & \mathbf{0} & \mathbf{M_s} & \cdot & \mathbf{0} \\ \cdot & \cdot & \cdot & \cdot & \cdot \\ \mathbf{0} & \mathbf{0} & \cdot & \cdot & \mathbf{M_s} \end{bmatrix} \quad \text{with} \quad \mathbf{M_s} = \begin{bmatrix} m_a & 0 \\ 0 & m_d \end{bmatrix} \tag{24}$$

where m_a and m_d are the modal masses of the blade and the corresponding disk sector, respectively. The stiffness matrix **K** is given by

$$\mathbf{K} = \begin{bmatrix} \mathbf{K^a} & \mathbf{K^b} & \mathbf{0} & \cdot & \mathbf{K^b} \\ \mathbf{K^b} & \mathbf{K^a} & \mathbf{K^b} & \cdot & \mathbf{0} \\ \mathbf{0} & \mathbf{K^b} & \mathbf{K^a} & \cdot & \cdot \\ \cdot & \cdot & \cdot & \cdot & \mathbf{K^b} \\ \mathbf{K^b} & \mathbf{0} & \cdot & \mathbf{K^b} & \mathbf{K^a} \end{bmatrix} \tag{25}$$

where

$$\mathbf{K^a} = \begin{bmatrix} k_a & -k_a \\ -k_a & k_a + k_d + 2k_c \end{bmatrix} \quad \text{and} \quad \mathbf{K^b} = \begin{bmatrix} 0 & 0 \\ 0 & -k_c \end{bmatrix}. \tag{26}$$

The proportional damping matrix is given by

$$\mathbf{C} = \alpha\mathbf{M} + \beta\mathbf{K} \tag{27}$$

where the proportionality factors α and β are 1.0823 and 7.6536×10^{-5}, respectively. The damping ratios for all modes are approximately equal to 0.01.

Mistuning is simulated by altering the stiffness (and hence the corresponding diagonal term of the stiffness matrix) of the blade by $\delta\mathbf{K^a}$, where

$$\delta\mathbf{K^a} = \delta_b \begin{bmatrix} k_a & -k_a \\ -k_a & k_a \end{bmatrix}. \tag{28}$$

The mistuning severity index, δ_b, is the percentage of stiffness reduction in the mistuned blade. To demonstrate the effect of mistuning, a bladed disk is simulated with the parameters given in Table 2.

3.2 Noise-free mistuning identification

To validate the proposed methodology, this section presents a parametric study on different mistuned blades and severities. Although a low level of mistuning is a minor level of damage, if unnoticed at an early stage it can lead to catastrophic failure. Therefore, the study focuses at the incipient level of mistuning of 0.5% severity. Also, it is important to investigate the mistuning severity up to 5% since small variations of material properties, geometric properties or manufacturing tolerances fall within this limit. This section highlights the versatility of the WEBMI by considering the identification of single and multiple mistuned blades, as given in Table 3.

In the numerical simulation, the bladed disk was excited with a short impulse with a duration of 10 ms, and the corresponding response was obtained for a period of two seconds from the two DOF model as presented in

Table 3 Different mistuned blades and severities without noise

Test case no.	Mistuned blade no.	Mistuning severity %
1	3	0.5
2	18	0.5
3	4, 16	0.5
4	3, 9, 17	0.5
5	3	0.5–5
6	18	0.5–5

Sect. 3.1. This study employed the response of both tuned and mistuned blades in the mistuning identification methodology as shown in Fig. 3. The mistuning was induced by reducing the stiffness by 0.5% of different blades as given in Table 3. Figure 5a–c shows the responses of three blades, when blade 2 was excited, including the responses of adjacent blades. The time responses of the tuned and mistuned cases reveal a slight change in the blade 3 response, whereas the symmetry in the response of blades 2 and 4 was conserved. Blades far from the mistuned blade showed no perceptible change in their response. However, it is difficult to draw a clear decision about the location of mistuning using only blade responses. Thus, the frequency response function (FRF) was obtained for the tuned and mistuned cases as shown in Fig. 5d. The 2-DOF model has two families of modes corresponding to the combined blade and disk sector response. The natural frequencies of the tuned blade and disk sector are 12.24 and 29.56 Hz, respectively. These values were reduced to 12.22 and 29.52 Hz for the mistuned blade and disk sector cases, respectively. The variation in natural frequencies can be suppressed by adding noise to the original signal. Therefore, the variation in natural frequencies may not be sufficient to ensure the identification of damage occurrence.

Hence, a robust mistuning identification algorithm was developed using the WPT which can identify the subtle changes that occur in the time response signal. The Haar wavelet has sharp discontinuous characteristics which can capture the subtle transient frequency changes in the signal [27]. Then, the time response of each blade was subjected to the WPT which was decomposed into different frequency bandwidth signals. The critical task of this analysis is to choose the optimal level of decomposition; hence, the Shannon entropy method was adopted, as briefly discussed in Sect. 2.4.2. Based on the method, the entropy of both approximate and detail coefficients was computed at each level. At the second decomposition level, the entropy was 1.7564×10^{-5}, which was less than the entropy of the detailed coefficients, which was 1.8071×10^{-5}; thus, the second level of decomposition was chosen to be an optimal level to identify small changes of 0.5% stiffness reduction in different blades. The wavelet packet energy was estimated at each node for the jth level of decomposition. Finally, the pth nodal energy was extracted to obtain the WEBMI, which is very sensitive to subtle changes due to crack induced mistuning of the bladed disk.

Figure 6a–d shows a small hump in the mistuning/damage zones for single and multiple blades for a severity of 0.5%. In order to ensure the exact mistuning location with a high confidence level, a threshold limit was applied to the WEBMI as discussed in Sect. 2.5. After subtracting the threshold limit $\mathrm{UL}^{\alpha}_{\mathrm{WEBMI}}$ from the WEBMI, the resulting WEBMI-$\mathrm{UL}^{\alpha}_{\mathrm{WEBMI}}$ show abrupt changes at the different single and multiple mistuned blades for the same level of severity (see Fig. 7a–d).

After achieving the first two levels of the mistuning identification strategy, the next stage was to estimate the mistuning severity. This study was focused only on mistuning due to manufacturing tolerances or variations in material properties or cracks. Thus, the parametric study was conducted for mistuning severities that varied from 0.5 to 5% in blades 3 and 18, which are test cases 5 and 6 given in Table 3. Figure 8 shows that the WEBMI increases monotonically as the mistuning magnitude increases for the mistuned blades. The WEBMI values for blades 3 and 18 also show a similar trend for the same amount of severity.

3.3 Mistuning identification with noise

In practical cases, the signals are highly contaminated with various noise sources, such as measurement noise or ambient noise. Hence, it is essential to test the mistuning index on noisy simulated data before applying the approach to experiments. Gaussian white noise was added to the simulated time response to give a series of uncorrelated random variables. The signal-to-noise ratio (SNR) value was chosen to be 1% in this study, which means that the signals are polluted with random noise to test the robustness of the WEBMI methodology. The noisy time responses for three blades are illustrated in Fig. 9, which are adjacent to mistuned blade 3.

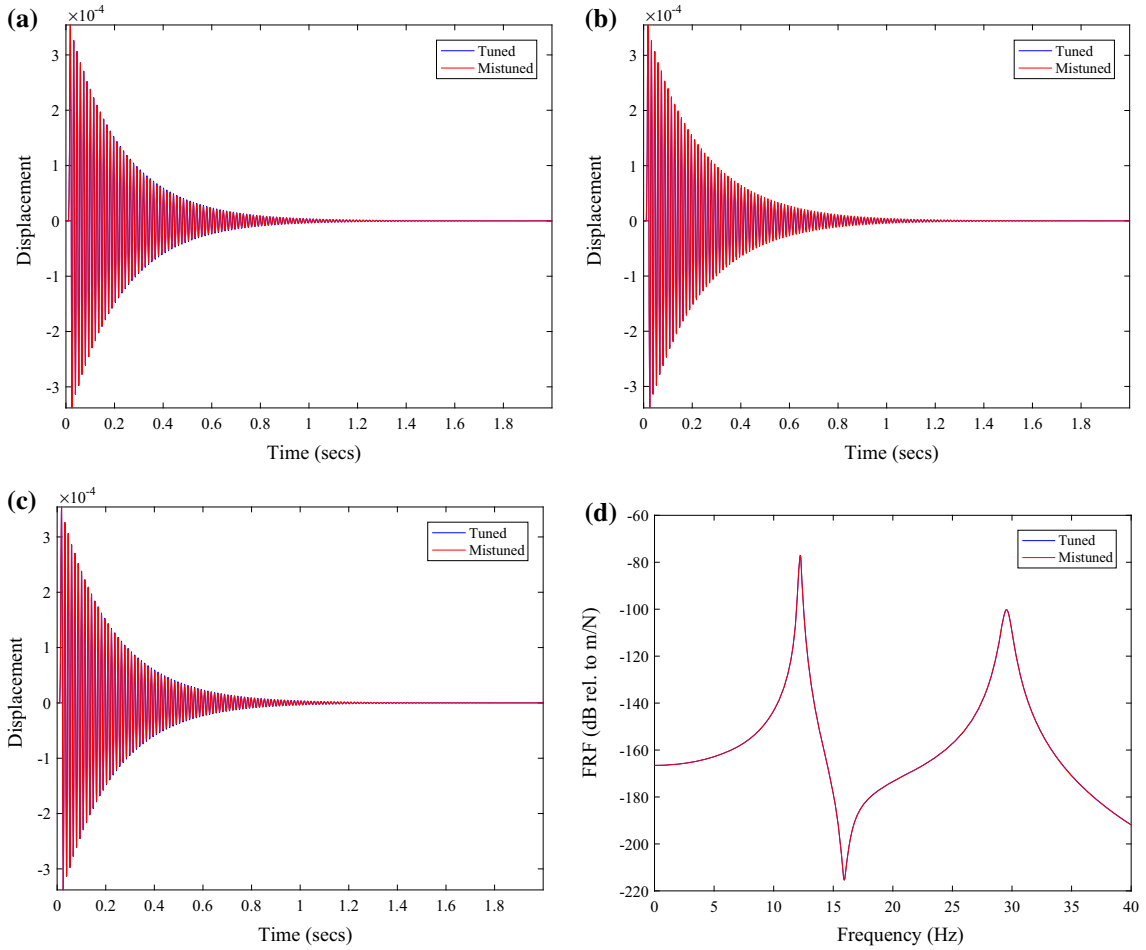

Fig. 5 Time responses of blades 2–4 due to mistuning in blade 3. Time response of **a** blade 2, **b** blade 3, **c** blade 4, **d** FRF of Blade 3

The noisy time responses were analyzed using the WEBMI methodology, which required the second level of decomposition to identify a mistuning severity of about 0.5% at blade 3, as shown in Fig. 10a. However, the WEBMI shows only a small change in the mistuned blade 3 due to noise contamination in the signals, which was not sufficient to identify the mistuned blade location. So the threshold limit was applied to the WEBMI, and the resulting WEBMI-$\text{UL}^{\alpha}_{\text{WEBMI}}$ indicates a distinct peak at mistuned blade 3, as shown in Fig. 10b. Some other peaks exist due to noise contamination in the signals, but these are at a significantly lower amplitude. Hence, this study shows that the WEBMI with threshold limit works well, even for very noisy signals.

4 Experimental test rig

4.1 Design of the bladed disk

The bladed disk was designed based on the idea of expecting a reasonable change of response due to mistuning caused by inhomogeneities in the blade material (e.g., cracks) or by adding a mass to the blade. Also the response was assumed to be concentrated in the lowest family of modes which is reasonably separated from the higher modes. Figure 11a shows the design of the bladed disk in the SolidWorks software. A detailed modal analysis simulation of the bladed disk was performed using the finite element analysis (FEA) commercial software COMSOL Multiphysics, to predict the test response. A bonded contact was assigned to the contact faces between the base of the blades and the grooves of the central disk. A cylindrical support boundary condition

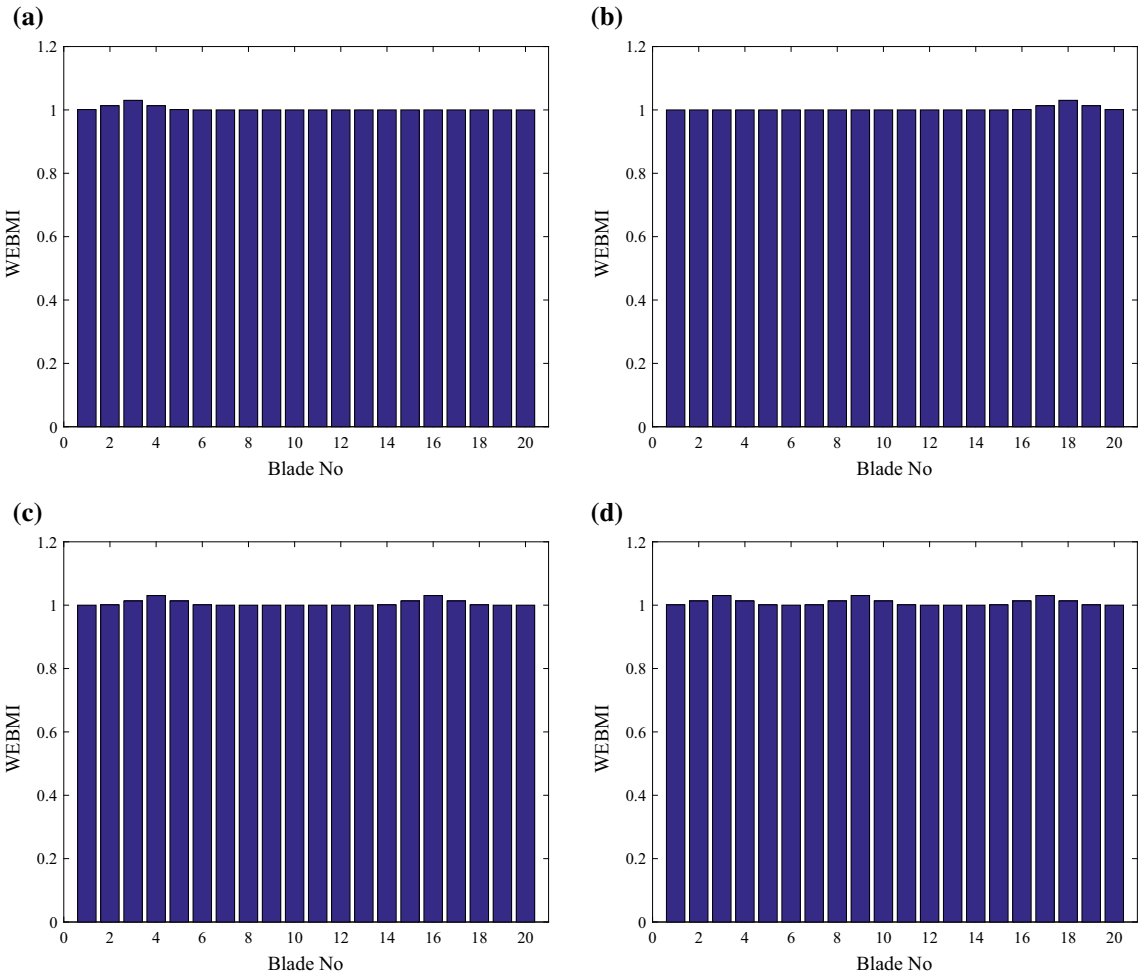

Fig. 6 The WEBMI for single and multiple mistuned blades with 0.5% mistuning at **a** blade 3, **b** blade 18, **c** blades 4 and 16, **d** blades 3, 9, and 17

was applied to the inner face of the disk, and finally a rotor speed of 50 rad/s was assigned to the disk. A modal analysis of the bladed disk structure was then performed.

Table 4 shows the first 24 natural frequencies of the bladed disk. The first twelve natural frequencies of the bladed disk structure are in a small range of frequencies [306–308 Hz], and this first family of modes are clearly separated from the higher modes. This first family of modes essentially comprise of first bending mode deformations of the blades. The second twelve natural frequencies comprise of a combination of torsion, second bending, and out of plane first bending modes of the blades. Figure 11b shows the mode shape corresponding to the first natural frequency.

4.2 Test rig description

An integrated test rig was designed and fabricated at Swansea University in order to validate the discussed technique. A detailed description is presented in this section. The test rig shown in Fig. 12 consists of a 60 mm diameter and 600 mm length horizontal shaft supported by two ball bearings fitted in two split plummer block housings. The shaft is driven by an AC servo motor with a maximum speed of 3000 rpm. A bladed disk attached to the end of the shaft is composed of 12 rectangular blades that are equally spaced. The 12 blades and the disk were wire cut from a thick steel block. A casing surrounds the bladed disk and will house the required sensors for blade tip timing measurements.

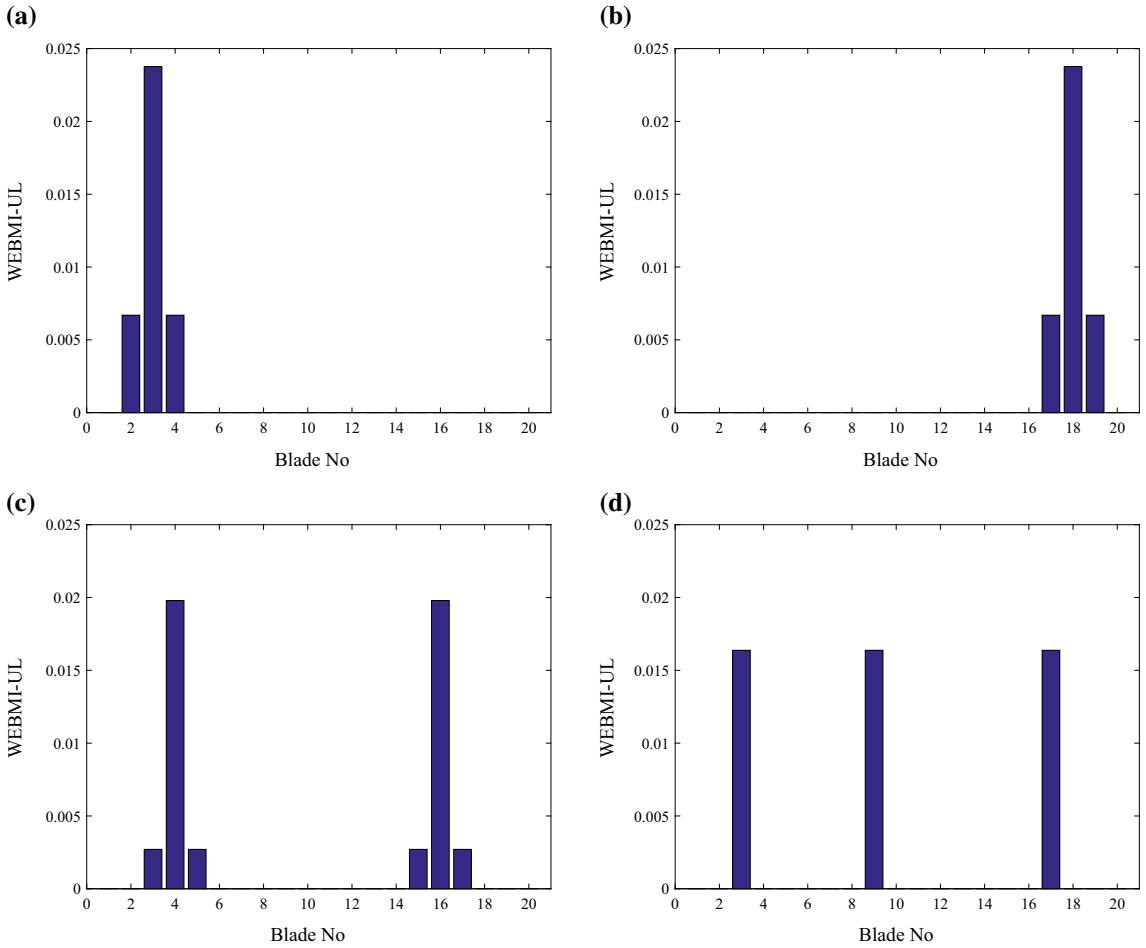

Fig. 7 The WEBMI-UL$^{\alpha}_{\text{WEBMI}}$ for single and multiple mistuned blades with 0.5% mistuning at **a** blade 3, **b** blade 18, **c** blades 4 and 16, **d** blades 3, 9, and 17

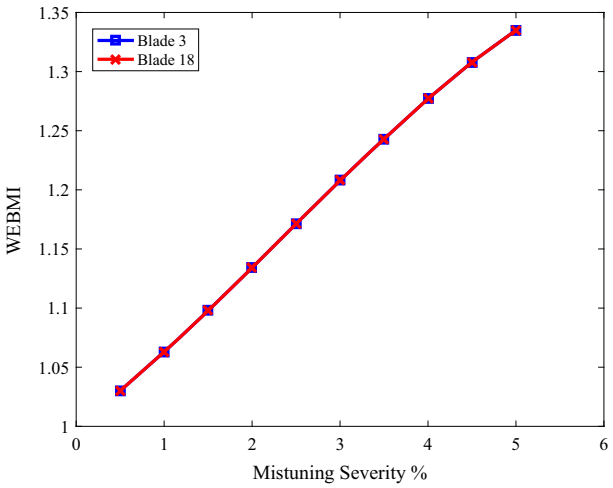

Fig. 8 Variation of the WEBMI for different mistuning severities at different blades

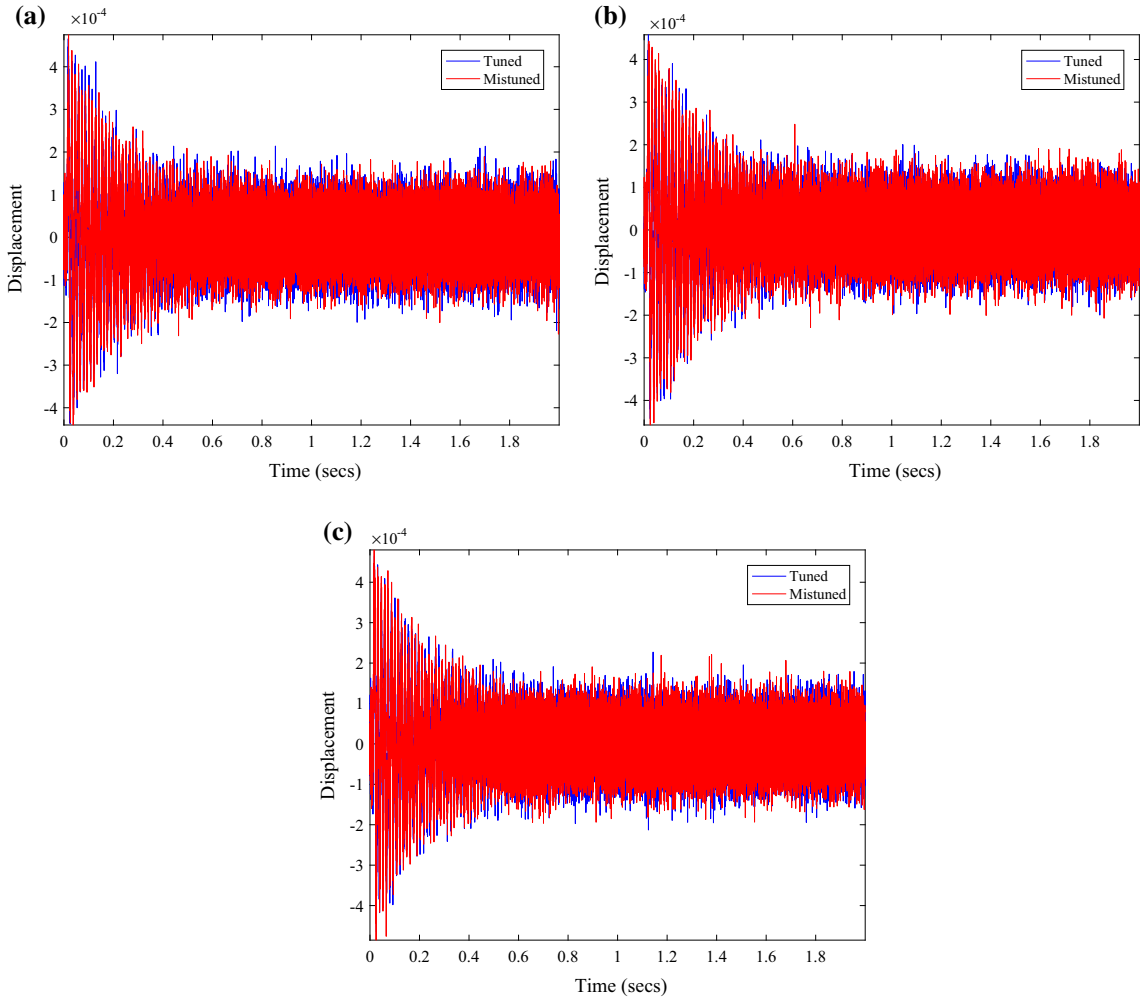

Fig. 9 Time responses of blades 2–4 due to mistuning in blade 3 with 1% SNR. Time response of **a** blade 2, **b** blade 3, **c** blade 4

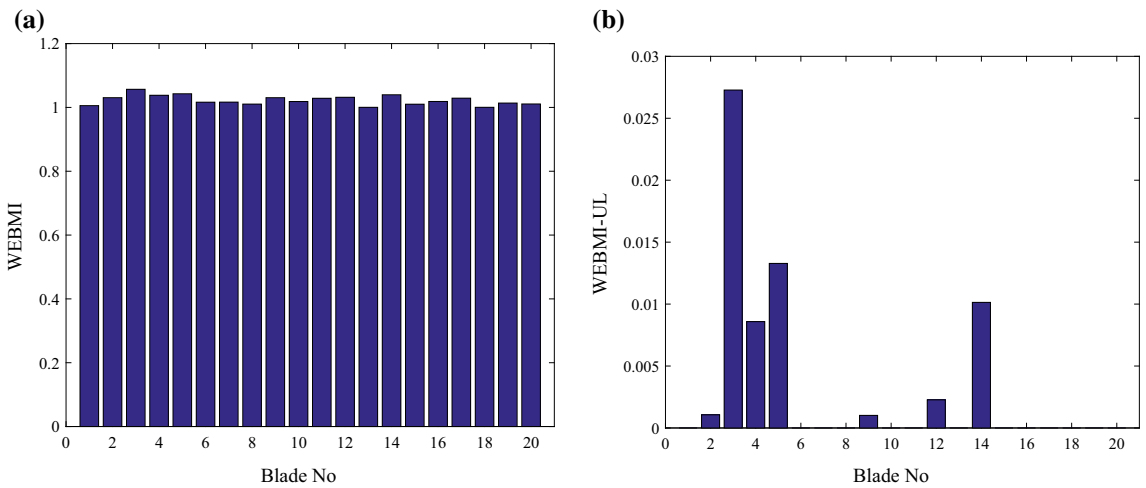

Fig. 10 **a** The WEBMI, **b** WEBMI-UL$^{\alpha}_{\text{WEBMI}}$ for 0.5% mistuning at blade 3 with 1% SNR

4.3 Hammer impact test

An impact hammer experiment was performed to test the proposed WPT algorithm discussed in Sect. 2. The manufactured bladed disk details are given in Sect. 4.2. To perform this experiment, a 4-channel data acquisition (DAQ) system, three accelerometers, an impact hammer, and data acquisition software were used. Due to the limited number of the DAQ channels, the 12 blades of the bladed disk were not monitored simultaneously, and so every three adjacent blades were analyzed separately. The details of the experimental setup are shown in Fig. 13a. The non-rotating blade was excited by the impact hammer, and the responses were measured at the tip of each blade by accelerometers, for three different blades simultaneously, as shown in Fig. 13b. An artificial approach was adopted to simulate mistuning in a blade. An extra mass was added to the blade to affect the dynamics of the blade; this is called a mistuned blade in Sect. 4.4. This approach is easier to treat experimentally than reducing the stiffness by cutting the blade. A magnet of 38 g mass was placed on the blade, as shown in Fig. 14.

The different test cases were performed on each set of 3 adjacent blades to validate the proposed WPT mistuning identification algorithm, are given in Table 5. The mistuning test cases were performed by changing the added mass locations along the same blade or moving it from one blade to another. The impulse excitation and time response samples were recorded through a 4-channel Data Physics DAQ system for a period of 3.2 s with a sampling rate of 2 kHz. The samples were averaged for 10 trials in order to obtain clean data.

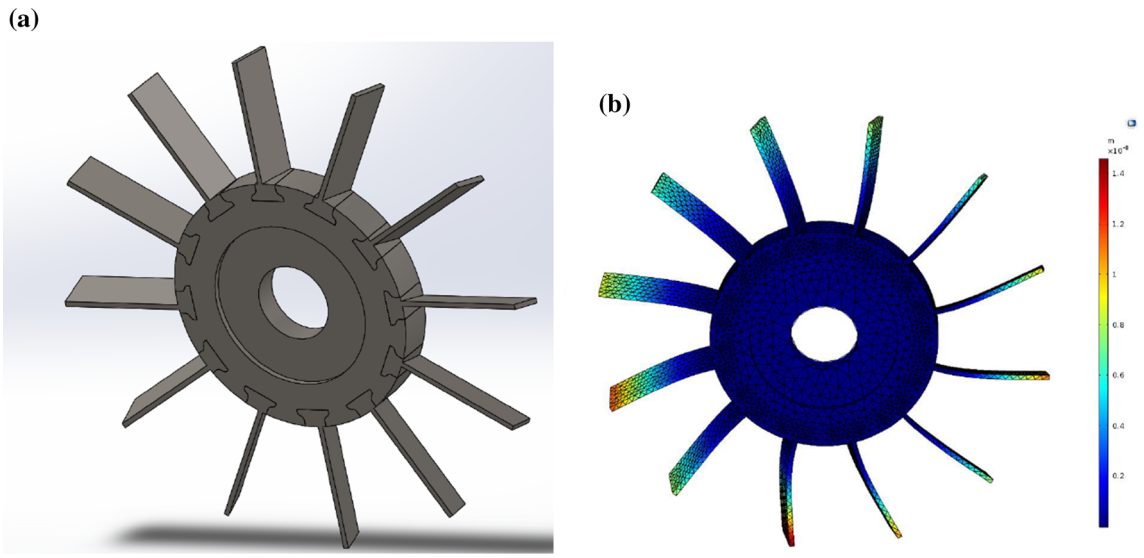

Fig. 11 **a** Design in SolidWorks, **b** the first mode shape of the bladed disk

Table 4 The first 24 natural frequencies of the bladed disk

Mode no.	Natural frequency (Hz)	Mode no.	Natural frequency (Hz)
1	306.78	13	1390.3
2	307.18	14	1390.4
3	307.24	15	1520.5
4	307.31	16	1596.8
5	307.34	17	1596.8
6	307.38	18	1905.6
7	307.4	18	1909.1
8	307.41	20	1909.1
9	307.44	21	1931.6
10	307.45	22	1931.8
11	307.45	23	1932.0
12	307.53	24	1932.1

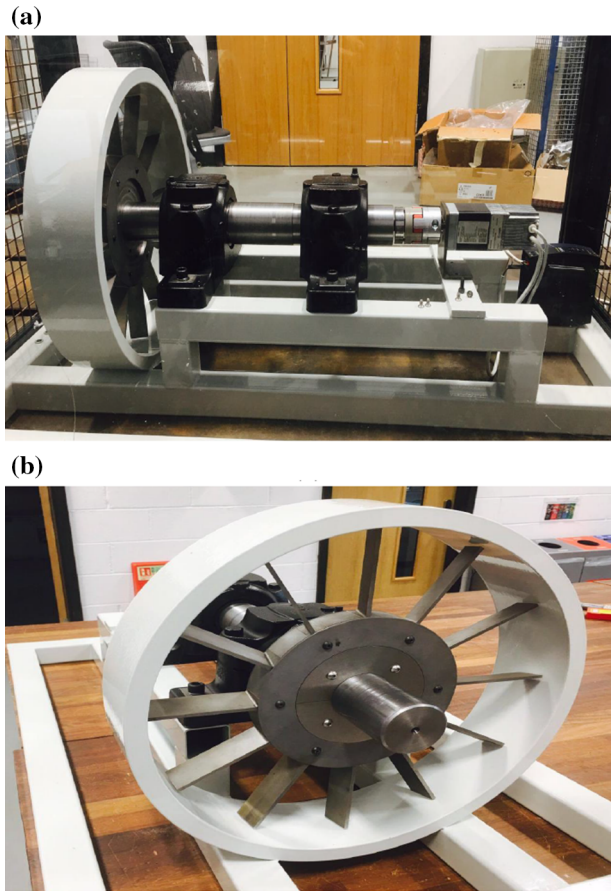

Fig. 12 **a** Full view of test rig, **b** front view of test rig

4.4 Experimental validation

Knowing that the impulse excitation is arbitrary, it is difficult to compare the responses between the tuned and mistuned case (e.g., without and with added mass). Therefore, normalization is essential before using the responses in the mistuning identification algorithm. Assuming that the free vibration analysis is linear, the acceleration response is proportional to the excitation and then it is normalized by the maximum excitation force. First, measurements were acquired when all blades were identical and no mass was added, i.e., the tuned bladed disk. The frequency response function (FRF) corresponding to this case is shown in Fig. 15. The first family of modes occurs in the range [280–310 Hz] which agrees with the calculated natural frequencies as mentioned in Table 4. The mode that appears in Fig. 15 at approximately 380 Hz is due to the rocking vibration of the rotating disk/shaft system.

The configuration corresponding to case 1 in Table 5 was then tested. The normalized time responses of the tuned and mistuned cases are shown in Fig. 16. It is clearly seen that the response amplitude of the tuned case is higher than in the mistuned case which is not predicted in the numerical simulation. This event occurs due to the arbitrary force applied on the structure. Also, the tuned response of case 1 showed the beat phenomenon due to very closely space modes. This phenomenon could not be captured by the simulation even though the 2-DOF model was considered. However, it is very challenging to identify the mistuning signature from the normalized responses between tuned and mistuned cases.

The FRFs for blades 1, 2, and 3 corresponding to tuned and mistuned cases were then obtained and are shown in Fig. 17. Figure 17a, c shows that there is no significant change in the FRF at blades 1 and 3 corresponding to the tuned and mistuned cases, whereas a small shift exists for blade 2 between the tuned and mistuned (added mass) cases, shown in Fig. 17b. Also, another peak exists away from the first mode for the mistuned cases in all three blades due to the addition of the added mass as shown in Fig. 17. There is also a slight increase in the frequency due to the stiffness addition for blade 2, which has a larger effect than

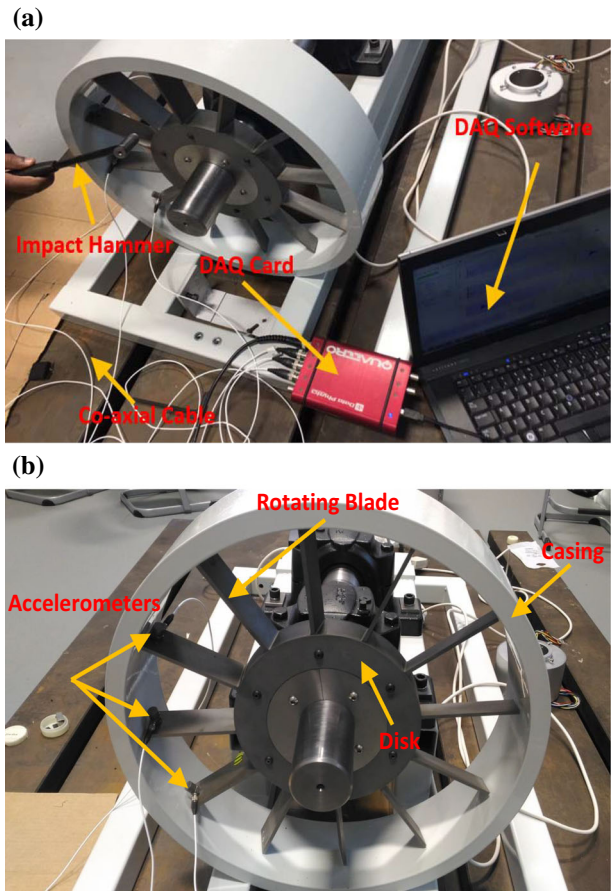

Fig. 13 **a** Impact hammer test setup, **b** front view of the setup

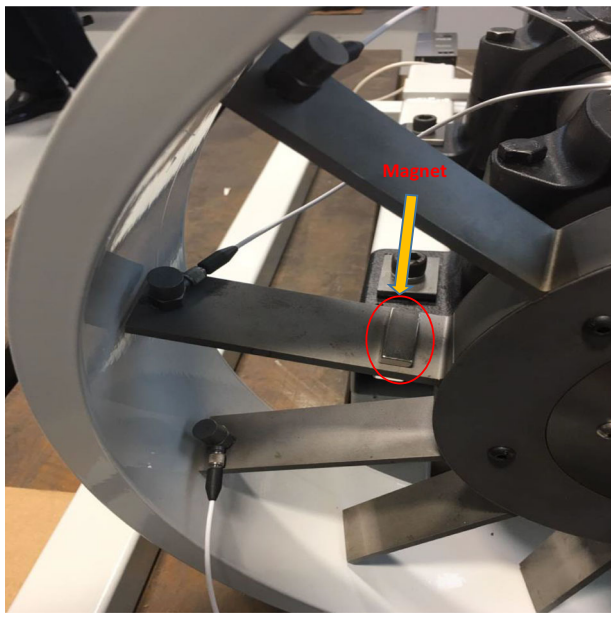

Fig. 14 Blade with added magnet mass

Table 5 Different test cases to simulate mistuning in blades

Test case no.	Mass added to blade no.	Added mass per blade (gms) (mistuning severity)
1	2	38
2	6	19
3	6	38
4	8 and 9	19

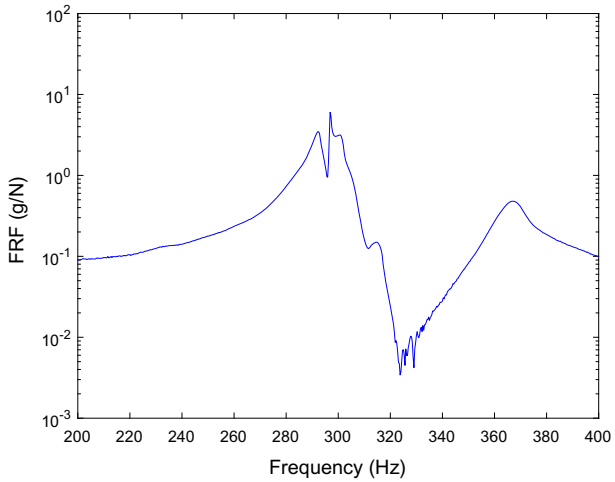

Fig. 15 Measured FRF corresponding to tuned blade no. 2

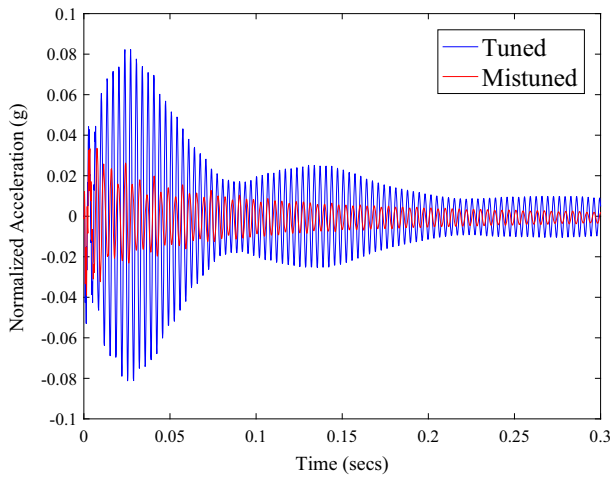

Fig. 16 Time responses of tuned and mistuned blade corresponding to case 1

the mass addition, as shown Fig. 17b. This frequency shift reveals the limited information that may identify the existence of mistuning but not location or severity. Similarly, the FRF data might give false identification of mistuning due to changes in boundary conditions, aliasing effects, etc. However, the time response has an ability to detect small changes in the response due to mistuning by applying the WPT algorithm. Thus, the normalized response corresponding to case 1 was subjected to the proposed WPT algorithm in order to estimate the WEBMI. The level of decomposition was chosen based on the Shannon entropy method as discussed in Sect. 2.4.2. The estimated entropy for the approximate coefficients was 0.1865, which was less than detail coefficients at 0.4247 for level 4. Thus, experimental case 1 required a level 4 decomposition to reveal the small variation of properties in the blade 2 response, as shown in Fig. 18a, which agrees with the configuration of case 1 by adding mass to blade 2.

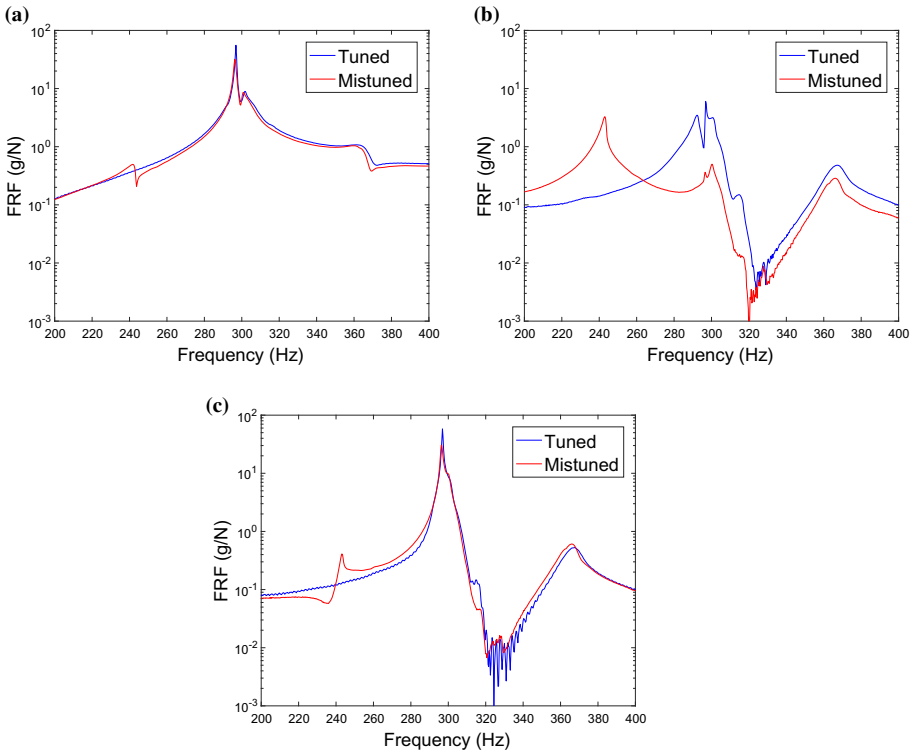

Fig. 17 FRF corresponding to case 1 of **a** blade 1, **b** blade 2, **c** blade 3

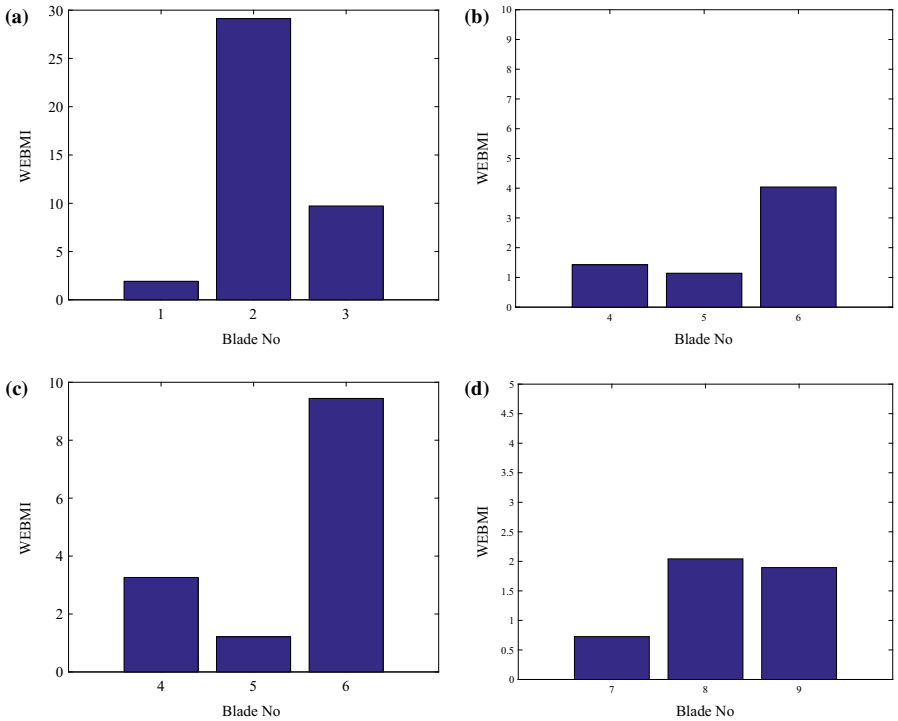

Fig. 18 WEBMI corresponding to **a** case 1, **b** case 2, **c** case 3, **d** case 4

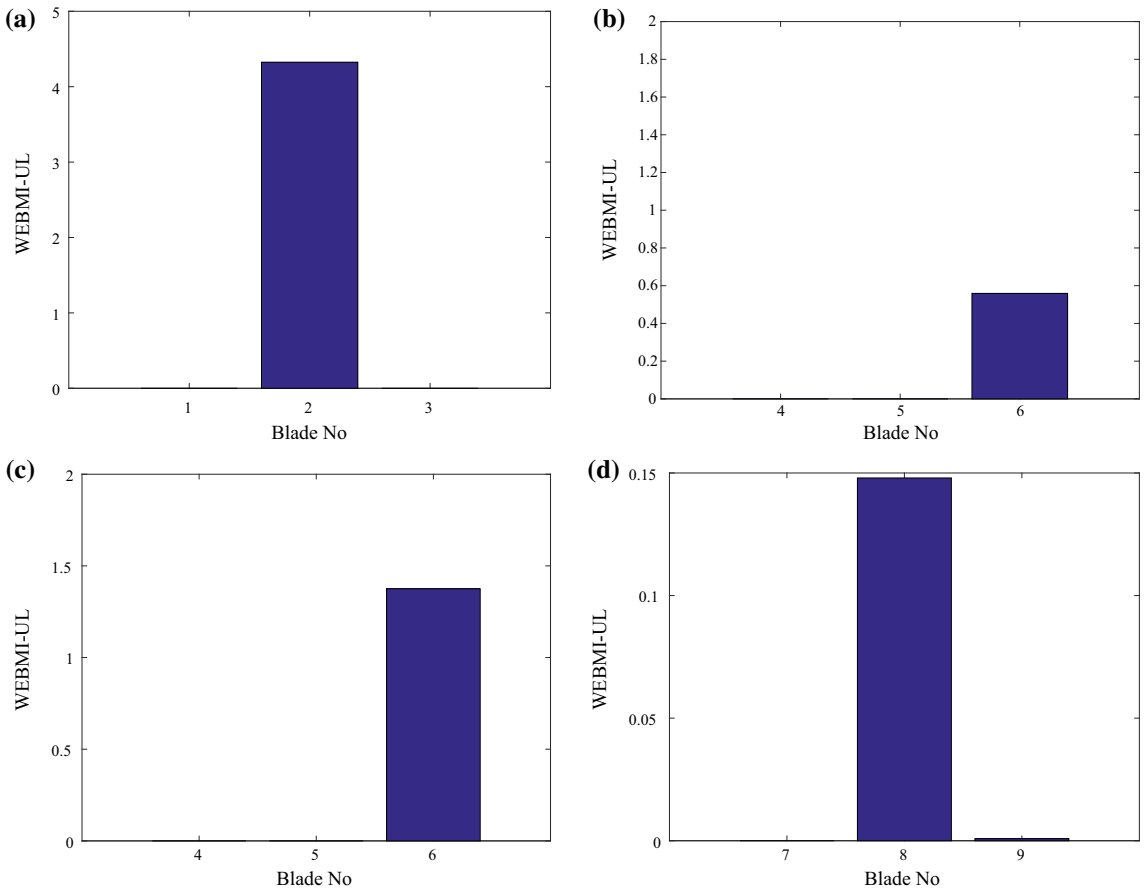

Fig. 19 WEBMI-UL$^{\alpha}_{\text{WEBMI}}$ corresponding to **a** case 1, **b** case 2, **c** case 3, **d** case 4

In the second and third cases, the stiffness and mass of blade 6 was altered, with one magnet for case 2 and two magnets for case 3, located close to the accelerometer. These two cases required the second level of decomposition to show the capability of the WEBMI to predict the increase of mistuning severity in cases 2 and 3, as shown in Fig. 18b, c, respectively.

In order to check the robustness of multiple mistuning locations, case 4 was performed by adding magnets to two adjacent blades (blades 8 & 9) as described in Table 4. This configuration required level 3 decomposition to determine the added mass locations on the different blades. Figure 18d shows the identification of mistuning in blades 8 and 9. To determine the exact mistuning location, a threshold was applied to the WEBMI as discussed in Sect. 2.5. Since each experimental case has only three samples or measurements, the threshold limit was estimated with low confidence. Even so, the identification of the location of mistuning is robust, as shown in Fig. 19a–d, and the experimental results have verified the robustness of the proposed method.

5 Conclusions

The paper has considered the identification of mistuning location and its severity in a bladed disk by a WPT technique. A two DOF lumped parameter model was employed to predict the fundamental dynamics of a bladed disk. The response of each blade was obtained from the two DOF model, and the WPT methodology was then applied. An optimal level of decomposition was determined using the Shannon entropy method, and the 'Haar or db1' wavelet was chosen. The numerical results of the WEBMI are sensitive to single and multiple mistuning in different blades. After implementation of the threshold limit to the WEBMI, the results of the WEBMI show abrupt changes to single and multiple mistuning as small as 0.5% in different blades. The WEBMI increases monotonically with the increase in mistuning severity, with the same trend for different mistuned blades. To check the robustness of the algorithm, Gaussian white noise with an SNR of 1% was added

to the response signal. The proposed algorithm is still reliable to detect the same magnitude of mistuning in different blades. Experiments were conducted to check the viability of the WPT methodology. Hence, the proposed index is a promising tool to detect incipient mistuning in bladed disks.

Acknowledgements The authors gratefully acknowledge the support of the Qatar National Research Fund through Grant No. NPRP 7-1153-2-432.

References

1. Meher-Homji, C.B., Gabriles, G.: Gas turbine blade failures—causes, avoidance, and troubleshooting. In: Proceedings of the 27th Turbomachinery Symposium (2007)
2. Castanier, M.P., Pierre, C.: Modeling and analysis of mistuned bladed disk vibration: current status and emerging directions. J. Propuls. Power **22**(2), 384–396 (2006)
3. Imregun, M., Ewins, D.: Aeroelastic vibration analysis of tuned and mistuned bladed systems. In: Proceedings of the Second Symposium on Unsteady Aerodynamics of Turbomachines and Propellers, Cambridge (1984)
4. Rzadkowski, R.: The general model of free vibrations of mistuned bladed discs, part I: theory. J. Sound Vib. **173**(3), 377–393 (1994)
5. Luo, R.: Free transverse vibration of rotating blades in a bladed disk assembly. Acta Mech. **223**, 1385–1396 (2012)
6. Rivas-Guerra, A.J., Mignolet, M.P.: Maximum amplification of blade response due to mistuning: localization and mode shape aspects of the worst disks. J. Turbomach. **125**(3), 442–454 (2003)
7. Castanier, M.P., Ottarsson, G., Pierre, C.: A reduced-order modeling technique for mistuned bladed disks. J. Vib. Acoust. **119**(3), 439–447 (1997)
8. Chatterjee, A., Kotambkar, M.S.: Modal characteristics of turbine blade packets under lacing wire damage induced mistuning. J. Sound Vib. **343**, 49–70 (2015)
9. Chatterjee, A.: Lumped parameter modelling of turbine blade packets for analysis of modal characteristics and identification of damage induced mistuning. Appl. Math. Model. **40**(3), 2119–2133 (2016)
10. Salhi, B., Lardiès, J., Berthillier, M., Voinis, P., Bodel, C.: Modal parameter identification of mistuned bladed disks using tip timing data. J. Sound Vib. **314**, 885–906 (2008)
11. Salhi, B., Lardiès, J., Berthillier, M.: Identification of modal parameters and aeroelastic coefficients in bladed disk assemblies. Mech. Syst. Signal Process. **23**, 1894–1908 (2009)
12. Yao, M.H., Zhang, W., Chen, Y.P.: Analysis on nonlinear oscillations and resonant responses of a compressor blade. Acta Mech. **225**, 3483–3510 (2014)
13. Yuan, J., Scarpa, F., Allegri, G., Titurus, B., Patsias, S., Rajasekaran, R.: Efficient computational techniques for mistuning analysis of bladed discs: a review. Mech. Syst. Signal Process. **87**, 71–90 (2017)
14. Hou, J.F.: Cracking-induced mistuning in bladed disks. AIAA J. **44**(11), 2542–2546 (2006)
15. Guru, S.S., Shylaja, S., Kumar, S., Murthy, R.: Pre-emptive rotor blade damage identification by blade tip timing method. J. Eng. Gas Turbines Power **136**, 072503-1 (2014)
16. Wang, S., Zi, Y., Li, B., Zhang, C., He, Z.: Reduced order modeling for mistuned centrifugal impellers with crack damages. J. Sound Vib. **333**, 6979–6995 (2014)
17. Hanachi, H., Liu, J., Banerjee, A., Koul, A., Liang, M., Alavi, E.: Bladed disc crack diagnostics using blade passage signals. Meas. Sci. Technol. **23**, 1–8 (2012)
18. Madhavan, S., Jain, R., Sujatha, C., Sekhar, A.S.: Vibration based damage detection of rotor blades in a gas turbine engine. Eng. Fail. Anal. **46**, 26–39 (2014)
19. Rioul, O., Vetterli, M.: Wavelets and signal processing. IEEE Signal Process. Mag. **8**, 14–38 (1991)
20. Wu, N., Wang, Q.: Experimental studies on damage detection of beam structures with wavelet transform. Int. J. Eng. Sci. **49**, 253–261 (2011)
21. Katunin, A.: Vibration-based spatial damage identification in honeycomb-core sandwich composite structures using wavelet analysis. Compos. Struct. **118**, 385–391 (2014)
22. Shahsavari, V., Chouinard, L., Bastien, J.: Wavelet-based analysis of mode shapes for statistical detection and localization of damage in beams using likelihood ratio test. Eng. Struct. **132**, 494–507 (2017)
23. Bagheri, A., Kourehli, S.: Damage detection of structures under earthquake excitation using discrete wavelet analysis. Asian J. Civ. Eng. **14**, 289–304 (2013)
24. Prakash, R., Srinivasan, S.M.: Rotational mode shape based added mass identification using wavelet packet transform. Int. J. Comput. Methods Eng. Sci. Mech. **16**, 182–187 (2015)
25. Rajendran, P., Srinivasan, S.M.: Identification of added mass in the composite plate structure based on wavelet packet transform. Strain **52**, 14–25 (2016)
26. Han, J., Ren, W., Sun, Z.: Wavelet packet based damage identification of beam structures. Int. J. Solids Struct. **42**, 6610–6627 (2005)
27. Capilla, C.: Application of the Haar wavelet transform to detect microseismic signal arrivals. J. Appl. Geophys. **59**, 36–46 (2006)
28. Jaffery, Z.A., Ahmad, K., Sharma, P.: Selection of optimal decomposition level based on entropy speech denoising using wavelet packet. J. Bioinform. Control **1**, 196–202 (2013)
29. Ang, A.H.S., Tang, W.H.: Probability Concepts in Engineering Planning and Design, vol. 1. Wiley, New York (1975)